

## DFT study of graphene antidot lattices: The roles of geometry relaxation and spin

Joachim A. Furst,<sup>1</sup> Thomas G. Pedersen,<sup>2</sup> Mads Brandbyge,<sup>1</sup> and Antti-Pekka Jauho<sup>1,3</sup><sup>1</sup>DTU Nanotech { Department of Micro- and Nanotechnology,  
Technical University of Denmark, DK-2800 Kongens Lyngby, Denmark<sup>2</sup>Department of Physics and Nanotechnology, Aalborg University, DK-9220 Aalborg East, Denmark<sup>3</sup>Department of Applied Physics, Helsinki University of Technology, P.O. Box 1100, FI-02015 HUT, Finland  
(Dated: February 21, 2024)

Graphene sheets with regular perforations, dubbed as antidot lattices, have theoretically been predicted to have a number of interesting properties. Their recent experimental realization with lattice constants below 100 nanometers stresses the urgency of a thorough understanding of their electronic properties. In this work we perform calculations of the band structure for various hydrogen-passivated hole geometries using both spin-polarized density functional theory (DFT) and DFT based tight-binding (DFTB) and address the importance of relaxation of the structures using either method or a combination thereof. We find from DFT that all structures investigated have band gaps ranging from 0.2 eV to 1.5 eV. Band gap sizes and general trends are well captured by DFTB with band gaps agreeing within about 0.2 eV even for very small structures. A combination of the two methods is found to offer a good trade-off between computational cost and accuracy. Both methods predict non-degenerate midgap states for certain antidot hole symmetries. The inclusion of spin results in a spin-splitting of these states as well as magnetic moments obeying the Lieb theorem. The local spin texture of both magnetic and non-magnetic symmetries is addressed.

PACS numbers: 73.63.Fg, 73.63.-b

## I. INTRODUCTION

Graphene, the single-atom thick two-dimensional sheet of carbon atoms, has stimulated considerable experimental<sup>1</sup> and theoretical research<sup>2</sup> as well as proposals for future nanodevices<sup>3</sup>. Various graphene-based applications have been realized in recent years<sup>4,5</sup> and the relevance for application in devices is heavily increased by the rapidly improving ability to pattern monolayers with e-beam lithography<sup>1</sup> where features on the ten-nm scale have been obtained<sup>6,7</sup>. Moreover, recent advances in chemical vapor deposition of graphene (see e.g. Ref. [8]) are promising for fabrication of large area, high quality devices.

Yet another way of nanoengineering graphene consists of defining an antidot lattice on graphene by means of a regular array of nanoscale perforations. This theoretical idea was introduced by Pedersen et al.<sup>9,10</sup>, who showed using tight-binding calculations that antidot lattices change the electronic properties from semimetallic to semiconducting with a significant and controllable band gap. Such structures have recently been realized experimentally by Shen et al.<sup>11</sup> and Eroms et al.<sup>12</sup> with lattice spacings down to 80 nm. Quantum dots and graphene ribbons have been demonstrated with dimensions of only a few nm<sup>13</sup>. Very recently, Girit et al.<sup>14</sup> have studied the dynamics at the edges of a growing hole in real time using a transmission electron microscope. Both in the experiment and in Monte Carlo simulations they find the zig-zag edge formation to be the most stable structure. This is in agreement with the findings of Jia et al.<sup>15</sup> who demonstrate a method to produce graphitic nanoribbon edges in a controlled manner via Joule heating. This opens the possibility of making antidot lattices

with a desired hole geometry.

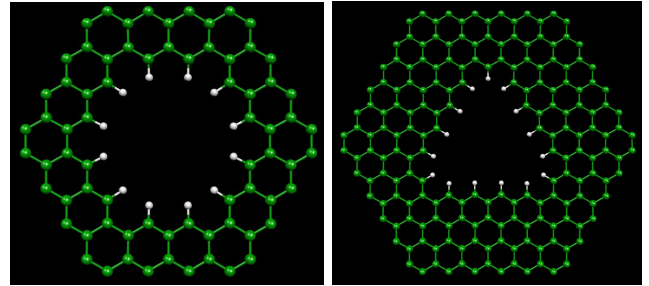


FIG. 1: (Color online) The unit cell of the  $f4/2g$  (left) and  $f6/5g4$  (right) system. The hexagonally shaped unit cells are repeated in plane to form a honeycomb lattice of antidots. The carbon atoms (green) are hydrogen terminated (white) along the hole edges.

While carbon nanotubes, graphene and recently graphene ribbons have been studied extensively using first principles methods, antidot lattices in graphene have mainly been treated with simpler models<sup>9,16</sup>. The very recent work by Vanevic et al.<sup>16</sup> uses a  $\pi$ -orbital tight-binding model to study antidot lattices with rather large lattice constants (these systems are more easily accessed experimentally but cannot be analyzed in terms of *ab initio* methods). Their focus is on the possible occurrence of midgap states without introducing defects in the antidot lattice, as was the case in the original proposal by Pedersen et al.

Many studies on magnetization have been reported for various graphene structures<sup>17,18,19,20,21,22</sup>. The origin of the magnetism can be understood based on the theory

by Lieb<sup>17</sup>, and the subsequent related work by Inui et al.<sup>23</sup> on the properties of the bipartite lattice. Single vacancies and their spin properties have been studied by, e.g. Lehtinen et al.<sup>18</sup> and Palacios et al.<sup>19</sup>; the latter paper also investigates voids in both graphene and graphene ribbons in detail using a mean-field Hubbard-model. Magnetization has also been studied in carved slits<sup>20</sup>, nite ribbons<sup>21</sup> and flakes<sup>21,22</sup> as well as rings<sup>24</sup> and notches<sup>25</sup>. Recently, DFT treatments of magnetic properties of nano-holes in graphene<sup>26</sup> and graphene InS<sup>27</sup> have been published.

The realized antidot lattices with hole sizes of several tens of nanometers and even larger lattice spacings involve several thousands of atoms in a unit cell and are computationally too costly to be treated with DFT in a systematic manner. The DFT based tight-binding method, DFTB<sup>28</sup>, however, allows one to address such large systems. The difference in computational cost between DFT and DFTB is for the present study found to be at least a factor of thirty. We thus investigate the accuracy of DFTB compared to DFT on much smaller antidot lattices in terms of the band structures<sup>32</sup>. Since geometry relaxation is the most costly task in DFT we also investigate the cost benefits of combining the two methods. By using DFT and elaborating on the role of spin, we also wish to address some of the main features found specifically for antidot lattices on a tight-binding level of the theory.

This paper is organized as follows. In Sec. II we introduce the antidot lattice systems and the methods used. The equilibrium geometries and band structures obtained using both DFT and DFTB and a combination thereof is given in Sec. III together with a detailed investigation of the spin properties. We conclude with a short summary.

## II. SYSTEMS AND METHOD

The specific realization of the antidot lattice we consider in this paper is a hexagonal (triangular) array of holes in a graphene sheet as proposed by Pedersen et al.<sup>9</sup>. Within the hexagonal unit cells there can be different hole geometries, and two examples of high symmetry holes are shown in Fig. 1. Below, geometries are fully relaxed but as a starting point ideal geometries using fixed bond lengths and angles of 120° are constructed. These geometries furthermore provide a straightforward notation for the structures. Thus, we designate antidot lattices with circular holes according to the notation  $fL;Rg$ , where  $L$  is the side length of the unit cell and  $R$  the hole radius, both measured in units of the graphene lattice constant  $a = 2.46$  Å giving a C-C bond length of 1.42 Å. Similarly, for triangular holes, we apply the notation  $fL;Dg$ , where  $D$  denotes the side length of the hole<sup>16</sup>. The holes are passivated with H using a C-H bond length of 1.1 Å and consist almost entirely of zig-zag edges. These structures are idealized but may well be within experimental reach given the recent advancements<sup>14,15</sup>.

Relaxation	DFT			Non-spin DFT	DFTB	
	None	DFT	DFTB	DFTB	None	DFTB
f4;2g	0.93	1.01	0.97	0.97	0.99	1.05
f5;2.8g	0.72	0.84	0.79	0.79	0.88	0.98
f5;3.5g	1.27	1.51	1.35	1.35	1.72	1.74
f6;3.6g	0.39	0.52	0.46	0.46	0.65	0.75
f6;5g <sub>4</sub>	0.24	0.22	0.22	0.00	0.00	0.00

TABLE I: The band gaps for various systems calculated with either DFT or DFTB using geometries obtained with different methods for relaxation. All values are in eV.

For the first principles calculations we have used the *ab initio* pseudopotential DFT as implemented in the Siesta code<sup>29</sup> to obtain the electronic structure and relaxed atomic positions from spin-polarized DFT<sup>33</sup>. We employ the GGA PBE functional for exchange-correlation<sup>30</sup>.

For the DFTB results<sup>34</sup>, we use the original (C,H) parametrization of Porezag et al.<sup>28</sup> which does not include spin.

## III. RESULTS

For all considered structures a structural relaxation with DFT leads to a shrinking of the hole, of the order of 1%, resulting in C-C bonds close to the edges stretching and contracting in the range of 1.39 – 1.45 (1.43 for f5;3.5g) Å. A few bond lengths away from the hole edge the C-C bond length remains unaltered at 1.42 Å.

In the case of relaxation with DFTB the picture is quite similar. Edge-atom C-C bond lengths vary from 1.39 – 1.42 Å for all systems but f6;5g<sub>4</sub>, which has variations of 1.38 – 1.44 Å. The shrinking of the hole size is smaller than 1%.

The results for the band gaps for five different systems are summarized in Table I. The band structures are calculated using both DFT and DFTB on structures relaxed at different accuracy levels and thus at different computational costs. The combinations are not exhaustive but represent a relevant set aimed at saving computational costs. The relaxation type is given in the second row of Table I. DFTB is expected to match DFT better as  $L=R$  increases due to decreased importance of edge details. The systems chosen here are mostly edge-dominated (low  $L=R$  ratio) and thus represent the worst case scenario.

Using DFT we find band gaps ranging from 0.2 to 1.5 eV confirming that the antidot lattice turns the semimetallic graphene into a semiconductor<sup>9</sup>. However, only spin-polarized DFT predicts a band gap for the f6;5g<sub>4</sub> structure which will be discussed in detail below.

Pedersen et al.<sup>9</sup> demonstrated a scaling-law between the hole size and the band gap for large  $L=R$  ratios but no such simple picture for small  $L=R$  ratios emerged. This

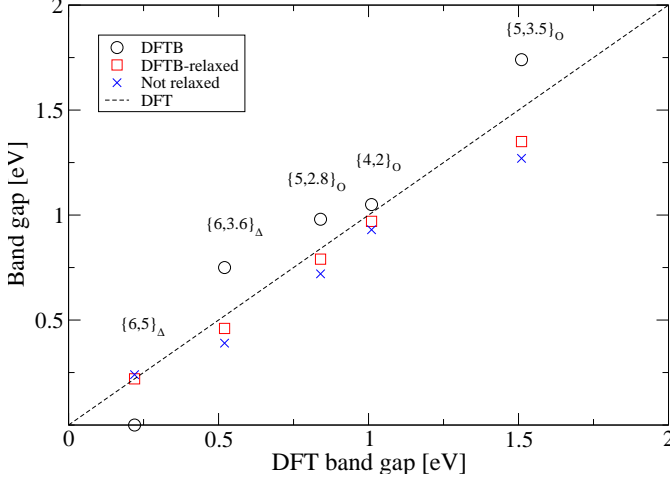


FIG. 2: (Color online) The band gaps for DFTB, DFT on DFTB-relaxed geometry and DFT on unrelaxed geometry plotted versus pure DFT results. Points above (below) the dotted line are thus overestimated (underestimated) compared to pure DFT. Note, that DFTB calculates the electronic structure without spin and fails to predict a band gap for the  $f6;5g_4$  structure.

trend agrees well with our edge-dominated systems were no simple scaling between the hole size and the band gap could be identified.

As illustrated on Fig. 2, DFTB in general gives a larger band gap than DFT (the circles lie consistently above the dashed line). This tendency is enhanced the more edge-like the structure becomes. On average, the DFTB gap is 20% larger than the DFT value for the four structures with circular perforations. The discrepancy increases for structures with holes occupying a large portion of the unit cell, such as  $f5;35g$ . Moreover, for  $f6;5g_4$  the omission of spin effects leads incorrectly to a vanishing DFTB band gap in agreement with non-spin DFT. In the cases of the  $f4;2g$  and  $f6;5g_4$  systems the band structures are shown in Fig. 3 left and right, respectively, calculated using DFT (DFTB) in the upper(lower) panel. We see that the shape of the bands corresponds qualitatively for the two methods.

#### A. Relaxation

We next analyze the importance of relaxation. The clear trend is that relaxation increases the band gap. This is illustrated for DFT in Fig. 2 (crosses corresponding to the unrelaxed structure lie below the dotted line), as well as in Table I for DFTB. Comparing unrelaxed results with fully relaxed results we see from Table I a change in band gaps within 10% and 15% using DFTB and DFT, respectively. Only in the case of DFT does the effect of relaxation increase the more edge-dominated the

system becomes. The change using DFT for the  $f4;2g$  system is 8% compared to 16% for  $f5;35g$ .

It must be emphasized that larger differences between initial and relaxed geometries may well give rise to a larger discrepancy between their band gaps. However, even for the case of a single passivated edge-defect the difference in relaxed and unrelaxed DFT band gaps is less than 10%.

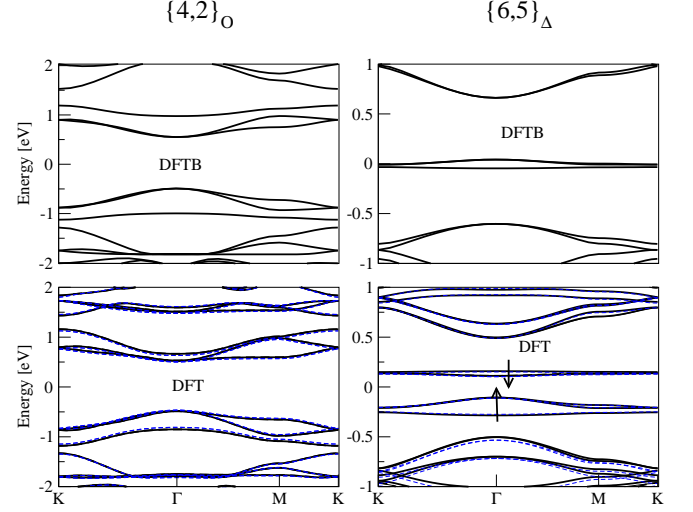


FIG. 3: (Color online) Band structures for the  $f4;2g$  (left column) and  $f6;5g_4$  (right column) system using DFTB (upper panels) and DFT (lower panels). The dotted blue curves in the lower panels are DFT results using structures relaxed with DFTB. The arrow pointing up (down) indicates that bands are filled with majority (minority) electrons only.

By relaxing the geometry with DFTB the DFT results are improved from the non-relaxed case as shown in Fig. 2 (the squares are closer to the dashed line than the crosses). Compared to pure DFT the largest difference in the band gap is again found for the edge-dominated  $f5;35g$  system: it is now 11% compared to 16% without relaxation. For the larger  $f6;5g_4$  structure we find the same values as for pure DFT. The DFT results are shown for both DFT-relaxed and DFTB-relaxed structures on Fig. 3 indicated by thick and dotted line, respectively. The different geometries do not change the bands notably.

Using DFT on DFTB-relaxed structures is thus an approach with a good trade-off between accuracy and computational cost. This finding is of great practical use, since relaxation is very costly in DFT.

#### B. Magnetic properties

For the  $f6;5g_4$  system with both non-spin-DFT and DFTB there are three (one nearly doubly degenerate) bands with weak dispersion at zero energy. Introducing

spin leads to a clear splitting of these bands, i.e., to the formation of a band gap. For a comparison of DFT and DFTB, see Fig. 3, right column. The three bands below (above) the Fermi level are half-filled by majority (minority) spin electrons and are thus completely spin-polarized. The size of the band gap is thus also an indication of the robustness of the magnetic state<sup>31</sup>.

The magnetic moments of the structures can be un-

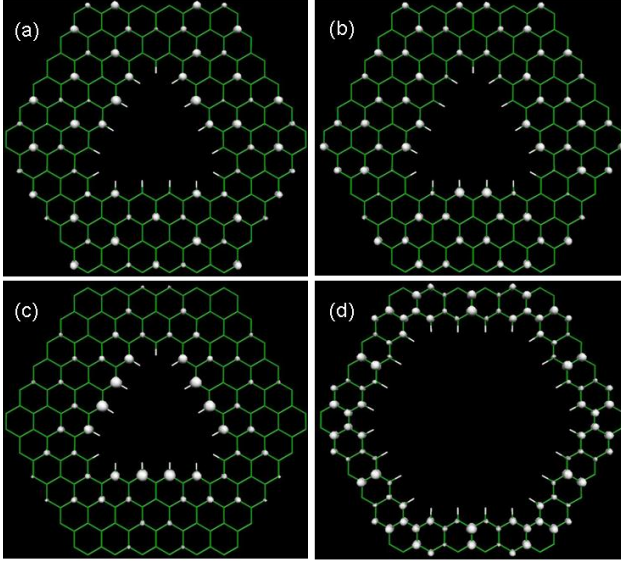


FIG. 4: (Color online) Amplitudes of certain important states. (a,b): degenerate midgap states, (c): non-degenerate midgap state of  $f6;5g_4$ , (d): highest filled bands of  $f6;3:6g$ . All states are calculated at the  $\Gamma$ -point.

derstood as a consequence of graphene being a bipartite lattice in the nearest neighbor approximation as shown by Lieb<sup>17</sup>. According to Lieb's theorem<sup>17</sup>, the total magnetic moment can be written as  $M = N_A - N_B$  where  $N_{A(B)}$  is the number of atoms occupying the A (B) sites of the bipartite graphene lattice. Thus, if the angle between the zigzag edges is 0° or 60° the edge-atoms belong to the same sublattice, while they belong to different sublattices if the angle is 120° or 180°. Consequently, the hexagonal hole is non-magnetic and the triangular is magnetic. This is consistent with a Mulliken analysis from the DFT calculations which shows a non-zero magnetic moment only for the  $f6;5g_4$  system of 3.00  $\mu_B$  per unit cell. By inspection of the geometry we indeed find  $N_A - N_B = 3$ .

As a continuation of Lieb's work, Inui et al.<sup>23</sup> showed that such sublattice imbalance results in there being  $N_A - N_B$  midgap states with zero energy. We thus expect a degeneracy of 3 of the low-dispersion bands in the  $f6;5g_4$  case.

In Fig. 3, lower right panel, there is one largely dispersionless band just below two almost completely degenerate bands which have some dispersion especially at the  $\Gamma$ -point. Such band curvature was also found for hydrogenated graphene ribbons by Kusakabe et al.<sup>31</sup> The

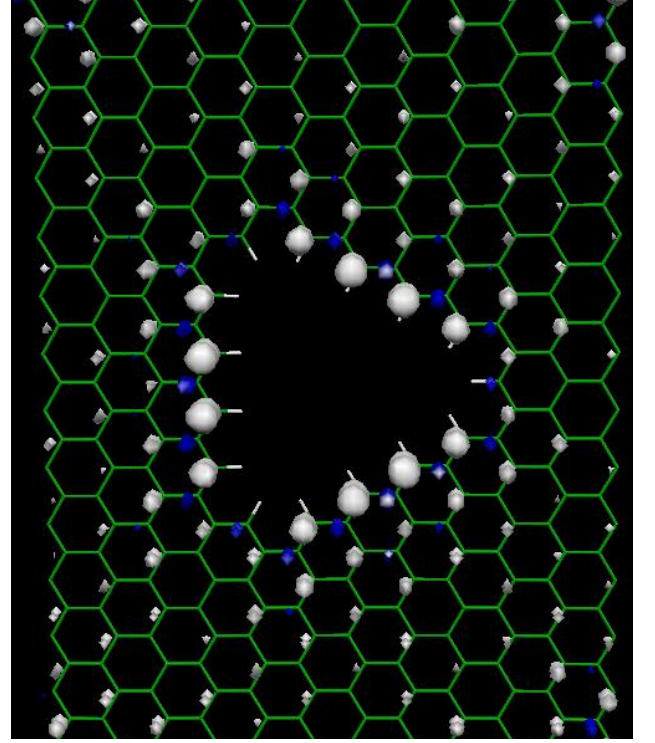


FIG. 5: (Color online) The difference in majority and minority spin densities for the  $f6;5g_4$  structure. Blue (white) indicates surplus of majority (minority) spin.

$\Gamma$ -point states for each band are shown in Fig. 4, where the strong localization is seen for the lowest band, Fig. 4(c), whereas the bands with curvature, Fig. 4(a,b), yield less localized states. Note also the alternation in the amplitudes of the states between sublattices as proposed by Inui et al.<sup>23</sup> The state of the highest occupied (spin-degenerate) band for the non-magnetic  $f6;3:6g$  structure is shown for comparison in Fig. 4(d). The splitting as well as the curvature is less pronounced for the unfilled states above the Fermi level showing particle-hole asymmetry. This asymmetry is expected due to the breaking of the symmetry of the bipartite lattice partly due to the DFT treatment beyond nearest neighbor as well as the passivation of the edges which changes the on-site potential at edge-sites. This is inherently also the case for DFTB. By inspection of the SIESTA Hamiltonian<sup>29</sup> we find an increase in on-site energy for passivated edge atoms as compared to atoms far from the edge. Vanevic et al.<sup>16</sup> find that a potential shift on the edge-atoms mainly causes a lifting of the degeneracy of the flat bands, consistent with our observations.

As mentioned above, the global spin is given by the sublattice imbalance. This does not, however, determine the local spin. For the hexagonally shaped hole structures we find not only a zero global spin, but also a zero spin on all atoms. This explains the identical band gaps found using DFT with and without spin. Such non-



